ACS APPLIED MATERIALS & INTERFACES

Research Article

www.acsami.org

Real-time and in Situ Drug Release Monitoring from Nanoporous Implants under Dynamic Flow Conditions by Reflectometric Interference Spectroscopy

Tushar Kumeria, Karan Gulati, Abel Santos, and Dusan Losic*

School of Chemical Engineering, The University of Adelaide, Adelaide, SA 5005, Australia

Supporting Information

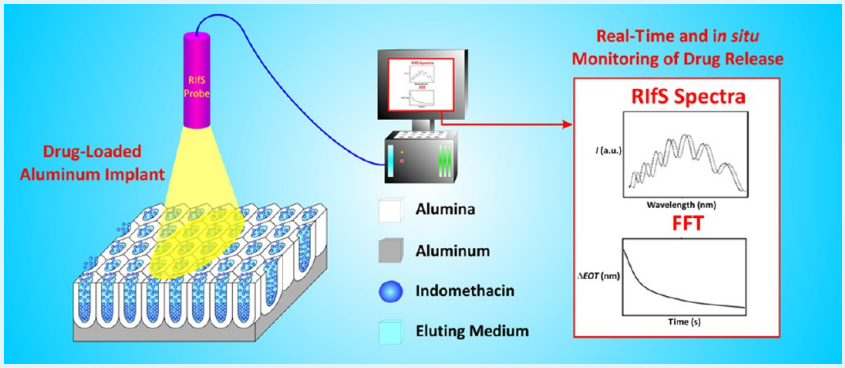

ABSTRACT: Herein, we present an innovative approach to monitoring in situ drug release under dynamic flow conditions from aluminum implants featuring nanoporous anodic alumina (NAA) covers used as a model of drug-releasing implants. In this method, reflectometric interference spectroscopy (RIfS) is used to monitor in real-time the diffusion of drug from these nanoporous implants. The release process is carried out in a microfluidic device, which makes it possible to analyze drug release under dynamic flow conditions with constant refreshing of eluting medium. This setup mimics the physiological conditions of biological milieu at the implant site inside the host body. The release of a model drug, indomethacin, is established by measuring the optical thickness change with time under four different flow rates (i.e. 0, 10, 30, and 50 μL min^{-1}). The obtained data are fitted by a modified Higuchi model, confirming the diffusion-controlled release mechanism. The obtained release rate constants demonstrate that the drug release depends on the flow rate and the faster the flow rate the higher the drug release from the nanoporous covers. In particular, the rate constants increase from 2.23 ± 0.02 to 12.47 ± 0.04 μg min$^{-1/2}$ when the flow rate is increased from 10 to 50 μL min^{-1}, respectively. Therefore, this method provides more reliable and relevant information than conventional in vitro drug release methods performed under static conditions.

KEYWORDS: *nanoporous anodic alumina, drug release control, dynamic flow conditions, nanoporous implants, optical thickness*

1. INTRODUCTION

Most current clinical therapies are based on intermittent oral or intravenous drug administration, which provide a high level of drug in blood right after the dose is administered. However, the drug level in the bloodstream immediately decreases. This is known as the peak-and-valley effect, which can generate many problems in clinical patients as the drug concentration in the bloodstream can reach toxic levels shortly after administration and subsequently fall below the therapeutic level, making the therapy inefficient. Furthermore, other inherent problems of these drug administration methods include low drug efficacy, poor bioavailability, and limited biodistribution. This has made these therapies unattractive for some clinical treatments like bone-related diseases (e.g., infection, cancer, osteoarthritis, etc.) as the blood supply is constrained by the poor perfusion in the bones, especially under traumatic conditions.[1−4] Another important issue to be accounted for increasing number of clinical patients with bone injuries/disorders like osteoporosis, severe fractures and cancers is our current lifestyle factors plus age-related conditions. In some cases, these patients require implants to support any bone structure for recovering partial or complete mobility. The benefits obtained from implants can be numerous although upon implantation these biomedical devices can lead to extensive inflammation, bacterial infection and poor implant-bone integration, which can ultimately lead to implant rejection/failure.[5−7] In this scenario, implantable local drug delivery systems are recognized to be the most attractive method to reduce implant-related problems and increase their integration in the host body. It is worth mentioning that local drug delivery systems also offer controlled and extended drug

Received: January 21, 2013
Accepted: June 3, 2013
Published: June 3, 2013

release, low dose requirement, and higher localized drug concentration, which reduce the disease treatment period.[8−10]

Recent advances in nanomedicine have enabled the use of several nanoporous materials including nanoporous anodic alumina (NAA), nanotubular anodic titania (NAT), and nanoporous silicon for local drug delivery administrations. These nanoporous materials are a promising alternative to other local drug delivery platforms (e.g. polymeric films and rubbers) as they neither erode nor degrade thus offer enhanced stability. Furthermore, these nanopores act as an efficient drug reservoir, which also allows a better control over the drug release kinetics.[11−15] Considerable research has been devoted in the past several years to study the applications of NAA and NAT as orthopedic, dental, coronary, and immunoisolation drug-releasing implants and chips, as a result of their chemical stability, controllable dimensions, tunable surface chemistry, high surface-to-volume ratio and biocompatibility.[12,13,16−19] Generally, the drug release performance of these structures is characterized through conventional in vitro batch monitoring process under static conditions (i.e., measuring the drug concentration from the UV−visible spectrum at fixed intervals of time).[20−22] Nonetheless, these systems cannot simulate dynamic in vivo conditions very closely as the eluting medium gets saturated of released drug after certain time. This reduces the concentration gradient between the bulk solution and the nanoporous implant (i.e. driving force) and significantly influences the release rate, making the results inaccurate. Therefore, there is an important lack of knowledge and understanding about the kinetics and mechanism governing drug release from nanoporous implants under dynamic flow conditions.[17,19,23] However, there is an increasing demand to develop localized drug delivery systems based on drug-releasing implants for its multiple advantages. To address this problem, new approaches have been recently reported to mimic the physiological conditions that prevail at the implant site in the host body. These systems used a continuous flow chamber in which the release kinetics of various antibiotics (i.e. amikacin, vancomycin gentamicin and tobramycin) from a poly-(methyl methacrylate) (PMMA) and calcium phosphate matrix were analyzed.[23−26] However, these techniques cannot be automated and multiple aliquots must be taken from the solution continuously throughout the whole release process, making the process labor intensive and less accurate for studying drug release mechanism within a short period of time (e.g. seconds or minutes).[17] To extensively monitor and understand the drug release kinetics, Gultepe et al. designed a fluorescence-based setup for monitoring in situ release of doxorubicin from nanoporous substrates in real-time. This setup acquired multiple readings over time without disturbing the release system, but was limited to fluorescent drugs or molecules under static conditions.[17]

To avoid the limitations of the systems described in the works just mentioned above, we designed a microfluidic device capable of accommodating a drug loaded nanoporous anodic alumina implant along with in situ drug release monitoring by a real-time technique as reflectometric interference spectroscopy (RIfS). This system combines both dynamic flow conditions and in situ drug release monitoring. RIfS is a versatile and highly sensitive detection technique based on the interference of white light reflected from a thin film. The detection principle is based on changes in the effective medium of the film, which can be easily monitored by measuring the effective optical thickness (EOT = $2n_{eff}L$), defined as the product between the effective refractive index of the film (n_{eff}) and its thickness (L).[27−30] Contrary to most of the current drug release monitoring systems, this system combines a microfluidic device, which makes it possible to maintain a high diffusion gradient between pores and eluting medium, with high resolution and real-time measurements of the released drug. This enables the study of drug release from nanoporous materials under physiological conditions. Indomethacin, an anti-inflammatory drug, is used as the model drug, whereas NAA is chosen as model of nanoporous substrate not only for its already proven capabilities (e.g., chemical and thermal stability, controllable dimensions and surface chemistry, biocompatibility, etc.), but also because it is highly optically active and generates well-resolved interference fringes.[31] To demonstrate the effectiveness of this system, we studied the effect of the flow rate of the eluting medium over the drug releasing performance of these NAA implants. This system simulates the drug diffusion from the nanoporous layer covering the implant to the surrounding tissues. Finally, the obtained results were validated and correlated both with experimental data obtained under conventional drug release conditions (i.e. static conditions) and theoretical values obtained from a modified Higuchi model in order to identify the mechanism of drug release.

2. EXPERIMENTAL SECTION

2.1. Materials. High-purity aluminum (Al) foils (99.997%) were supplied by Alfa Aesar (USA). Oxalic acid, ethanol (ChemSupply, Australia), chromic acid (Mallinckrodt, USA), phosphoric acid, and indomethacin (Sigma-Aldrich, Australia) were used as received. High-purity water was used for all solution preparation as produced by sequential treatments by Millipore system and a final filtering step through a 0.22 μm filter.

2.2. Preparation of NAA Implants. A two-step electrochemical anodization process was used to fabricate NAA with structurally engineered geometric characteristics as reported elsewhere.[32] Briefly, Al foils 1.5 × 1.5 mm^2 were sequentially sonicated in ethanol (EtOH) and distilled water for 15 min and dried under a nitrogen stream. First anodization was carried out in an aqueous solution of oxalic acid 0.3 M ($H_2C_2O_4$) at 6°C and 50 V for 10 h. Then, the resulting nanoporous anodic alumina layer was removed by wet chemical etching in an oxide removal solution (i.e., chromic acid 0.2 M (H_2CrO_4) and phosphoric acid 0.4 M (H_3PO_4)) for 3 h at 60 °C. Next, pre-textured Al substrates obtained by this process were subjected to final anodization, which was carried out for 40 min under the same conditions to obtain self-ordered nanopores, the pore diameter and length of which were approximately 30−35 nm and 4.5 μm, respectively.

2.3. Drug Loading and Release through Conventional Method. NAA substrates were loaded with an ethanolic solution of indomethacin 1% w/v by three different loading methods reported elsewhere:[21,22] (i) method 1, drug loaded inside the pores and on the NAA surface; (ii) method 2, drug loaded exclusively inside the NAA pores; and (iii) method 3, drug loaded only on the NAA surface. In method 1, 10 μL of drug solution were dropped onto the NAA substrates and allowed to dry by evaporation so that the drug solution wetted the pore walls as well as the top surface of the NAA substrate.

Method 2 was achieved by dropping the same amount of drug onto the NAA substrates but cleaning its surface by soft wiping and plasma cleaning treatment (plasma system ATTO, Deiner Scientific, Germany) to remove the excess of drug from the NAA surface. In method 3, 10 μL of drug solution was dropped onto the NAA substrates and evaporated in an oven at 80 °C under air atmosphere. In this way the solvent was evaporated before the drug solution wetted the pore walls. These loading processes were repeated 10 times to obtain an equivalent amount of drug loading in all the NAA implants.

To determine the amount of drug loaded into these NAA substrates, we performed a thermogravimetric analysis (Hi-Res

Modulated TGA 2950). First, the correct characteristic temperature peak for indomethacin decomposition was determined by heating 25 mg of pure drug in the platinum pan of the TGA balance from 20 to 800 °C. The drug peak was identified and used to calculate the total amount of drug present in the NAA substrates. The total drug loadings obtained by methods 1, 2, and 3 were established by averaging the resulting amount of drug in three different NAA implants, respectively.

Conventional in vitro drug release from NAA implants was investigated through changes in the UV-visible absorbance with time (Cary 60 spectrophotometer, Agilent Technologies, Australia). Briefly, NAA implants loaded with drug were immersed in 5 mL of PBS (pH 7.4) under static conditions. One milliliter of this solution was extracted for UV−visible characterization and replaced by 1 mL of fresh PBS after every measurement. First, measurements were taken at short intervals of 5 min during the first 100 min to monitor the initial drug release. After this, measurements were performed every 24 h until the total amount of drug was released into the eluting medium. These absorbance measurements were carried out at a wavelength of 320 nm, which is the characteristic absorbance wavelength for indomethacin. All the drug release measurements were repeated 3 times and statistical analysis was performed.

2.4. Flow Cell for in Situ Drug Release from NAA Implants. An unbounded microfluidic flow cell was fabricated in two reusable halves with a top glass cover and a microstructured base chip. The base chip was fabricated by hot embossing of the microstructure in solid PMMA. A brass stamp machined by a CNC micromachining (Supermill-2M, Kira, Japan) was replicated by embossing under pressure at 4.3 MPa and 130 °C in a hot embosser-substrate bonder (EVG, 520-HE, USA). The resulting microstructure consisted of two microchannels (i.e., single inlet-single outlet and triple inlet-single outlet), with the width and depth of 200 and 100 μm, respectively. These microchannels delivered the fluid into a 36 mm^2 cavity of 200 μm depth to accommodate 100 μm thick NAA implants. Hence, a further 100 μm space was left above the NAA substrate to allow the eluting medium to pass through the cavity without obstructions. Furthermore, an array of micropillars before the cavity chamber enabled an even distribution of the fluid over the NAA surface (see Figure S1 in the Supporting Information). These two halves of the microfluidic device (i.e. base chip and cover glass) were sealed together by a clamp, which allows the integration of the optical probe for RIfS measurements. Fresh PBS solution was flown through the system by a syringe pump (Fusion touch, Chemyx, USA). The flow rate was modified from 0 to 50 μL min^{-1} according to the reduced diffusion around bones in the physiological milieu (i.e. target soft tissues for these drug eluting implants). The blood flow rate calculated for cortical and cancellous bones in 20 weeks old pigs are up to 7.5 and 21.3 mL min^{-1} per 100 g of tissue, respectively.[23] The intension behind using these flow rates was not only to closely imitate the blood flow conditions observed per gram bone tissue of a 20 week old pig but also to maintain the constant concentration gradient between NAA implant and eluting medium.

2.5. RIfS Setup for in Vitro Release Monitoring. RIfS measurements were performed in a setup composed of a Y-junction optical fiber probe. One end of this optical probe was connected to a tungsten halogen light source (LS-1LL, Ocean Optics, USA) and the other end to a miniature spectrophotometer (USB 4000, Ocean Optics, USA). The common end of the probe was used to focus white light from the source and collect the reflected light from the drug-loaded NAA implants in the microfluidic cell. The obtained data were collected from an illuminated circular spot of 3 mm in diameter while the spectral range was 400-900 nm. For in situ monitoring of drug release, RIfS spectra were saved at an interval of 10 s with an integration time of 20 ms. The effective optical thickness (EOT) was obtained by applying Fast Fourier Transform to the RIfS spectra in Igor Pro library (Wavemetrics, USA). The release of indomethacin from these NAA implants was monitored through changes in effective optical thickness at different flow rates (i.e., 0 to 50 μL min^{-1}). All the in situ measurements were repeated 3 times and the obtained data were statistically analyzed.

2.6. Characterization of NAA Implants. The structural characteristics of NAA substrates such as pore diameter and thickness were established by image analysis from scanning electron microscopy (SEM) images (FEI Quanta 450, Japan). All samples for SEM characterization were coated by a 5 nm platinum layer before analysis.

3. RESULTS AND DISCUSSION

3.1. Structure and Morphology of NAA Implants. The geometric characteristics of the prepared NAA implants were established by scanning electron microscopy (SEM). Figure 1 shows a set of SEM images of the top surface and cross-sectional structure of resulting NAA implants after a two-step anodization process. These presented self-ordered and vertically aligned cylindrical pores with hexagonal arrangement, the pore diameters and lengths of which were 35-40 nm

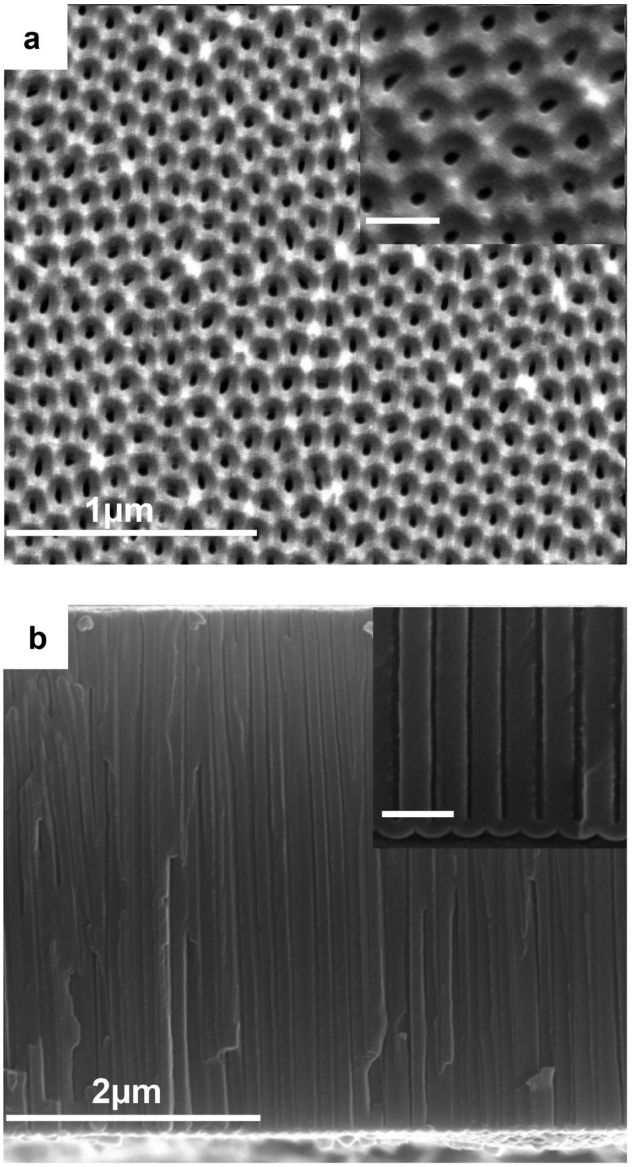

Figure 1. SEM images of prepared NAA substrates used as drug-releasing implants. (a) Top view showing hexagonally arranged pores with a high-magnification image in inset (scale bar = 100 nm). (b) Cross-section view with straight nonbranched pores with inset showing the oxide barrier layer at the bottom of the pores (scale bar = 100 nm).

(Figure 1a) and 4.5-5.0 μm (Figure 1b), respectively. The pores were closed at their bottom with an oxide barrier layer and thus capable of acting as a reservoir for drug molecules. The geometric characteristics of these NAA substrates were structurally engineered to hold a substantial amount of drug inside the pores with optimized optical response for RIfS measurements.[31]

3.2. Drug Loading and Release Monitored by Conventional Methodology. A set of thermogravimetric analyses (TGA) were performed on NAA implants loaded with indomethacin by methods 1, 2, and 3 to determine the total amount of drug loaded by different loading strategies. The weight change from 200 to 375°C was associated with the decomposition of pure indomethacin. According to the obtained weight reduction curve, we found that the total amount of drug loaded was 68 ± 11 μg, 53 ± 6 μg and 71 ± 9 μg for loading methods 1, 2 and 3, respectively (see Figure S2 in the Supporting Information). The amount of drug loaded in these NAA substrates by all the loading methods (i.e., method 1, method 2, and method 3) is summarized in Table S1 in the Supporting Information.

Figure 2 summarizes the results obtained for drug release experiments carried out by the conventional method under

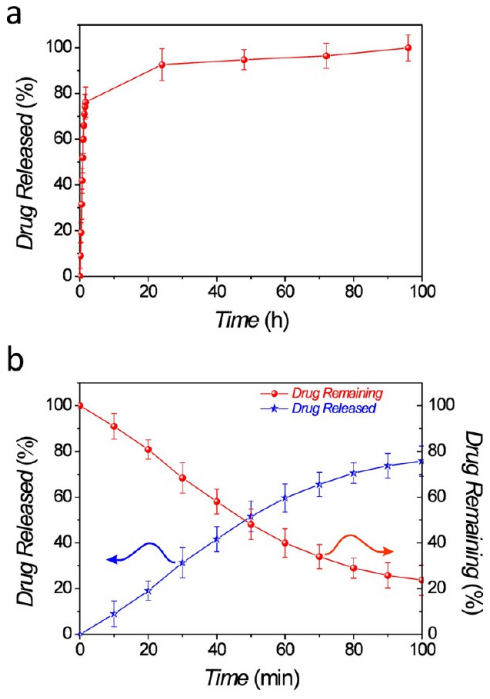

Figure 2. Drug release plots from NAA implants under static conditions (error bars correspond to standard deviations obtained after averaging 3 measurements). (a) Release pattern for the complete drug release during 4 days. (b) Amount of drug released (left scale) and amount of drug remaining in pores (right scale) during the first 100 min of release.

static conditions. The drug release pattern shown in Figure 2a can be described in two phases: namely, (i) an initial fast release of drug and (ii) a slow sustained release for 4 days in the course of which 100 % of the drug is eluted from the nanoporous implant. Initial release of indomethacin during the first 100 min is illustrated in Figure 2b. This verifies that around 75% of the total amount of drug was released from the NAA implant (i.e., 50 ± 4 μg) after 100 min. The initial release phase is related with a fast diffusion of the freely available loosely bound superficial drug molecules from the NAA implant surface because of the high concentration gradient of drug between the NAA implant and the eluting medium (i.e. phosphate buffer saline (PBS) solution). Nevertheless, a different pattern of drug release was observed after the 1st day of release, reaching a very slow release rate over the following 4 days. Approximately 1.6 μg of drug were released after 24 h from day 1 till day 4 of the release experiment. Hence, the drug release followed a linear trend in cumulative drug release amount. Notice that the release kinetics of this phase is controlled by the diffusion of drug molecules along the pores to the bulk eluting medium at the surface of the NAA implant.

3.3. Drug Release under Dynamic Flow Conditions Monitored by RIfS. Drug release from NAA implants under dynamic flow conditions was performed in a specially designed microfluidic cell, which made it possible to monitor the drug release in real-time and in situ conditions by RIfS. The optical thickness change was used as the sensing parameter to measure the concentration of released drug molecules from the NAA pores. Fresh PBS was flowed through the device at 30 μL min^{-1} not only to mimic biological fluid circulation inside the host body but also to maintain a high concentration gradient of drug between the NAA pores and the eluting medium. Figure 3

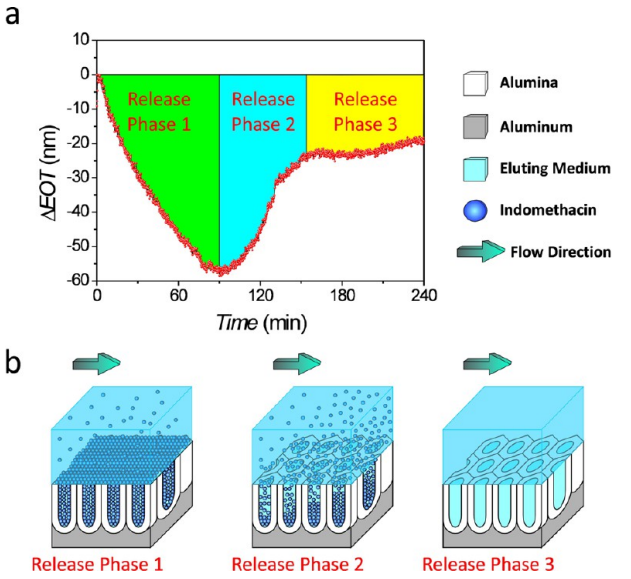

Figure 3. Relationship between ΔEOT with time and different drug release phases under dynamic conditions (flow rate = 30 μL min^{-1}). (a) ΔEOT change with time and different release phases. (b) Schematic diagram showing the evolution of drug release with time from the NAA implants under dynamic conditions.

shows the release pattern obtained through the effective optical thickness change (ΔEOT) generated by the release of drug from the NAA implants for 240 min. The release curve obtained by RIfS consists of three characteristic phases: namely, (i) an initial decrease in ΔEOT, (ii) an increase in ΔEOT, and (iii) final constant value of ΔEOT.

The initial release of drug and the decrease in ΔEOT are ascribed to the fast diffusion of drug molecules residing on the NAA surface. ΔEOT decreases for 100 min and starts to increase after this point. This increment is thought to be related with the drug release from the pore walls to the PBS solution inside the pores, which increases the refractive index of the

dx.doi.org/10.1021/am4013984 | ACS Appl. Mater. Interfaces 2013, 5, 5436−5442

effective medium. This suggests that this second phase is limited by drug diffusion from pores as result of drug-surface interactions. Finally, ΔEOT reaches a stable value, which corresponds to the NAA implant in PBS. This denotes that the drug has been entirely released from the NAA implant.

A set of control tests was carried out in order to confirm our hypothesis about the relationship between the observed drug release pattern and ΔEOT (see Figure S3 in the Supporting Information). The first control test was performed with a NAA implant loaded by Method 2 (i.e. drug only inside the pores). It was observed an initial decrease in ΔEOT for the first 3 min of release followed by a noticeable increment until Δ*EOT* reached a stable value in approximately 15 min at a flow rate of 50 μL min^{-1} (see Figure S3a in the Supporting Information). The results clearly confirmed that this release pattern is related to diffusion of drug molecules from the pores. Although some amount of drug still remained on the NAA implant surface after surface cleaning by physical and plasma cleaning treatment, this can be considered almost negligible. A second control test was performed with a NAA implant loaded with drug by Method 3 (i.e., drug loaded exclusively on the NAA implant surface). These results show that ΔEOT decreases throughout until it reaches a constant value. No increment of Δ*EOT* was observed after that, demonstrating that the drug release takes place only from the NAA implant surface and not from its pores (see Figure S3b in the Supporting Information). The aforementioned control experiments justified the triphasic release pattern presented in Figure 3.

Optimal drug dosage and release rate under dynamic conditions (i.e. similar to physiological milleu at implant site) is an esential requirement for drug-relasing implants used in any specific therapy. These characteristics cannot be established by means of conventional drug-relase monitoring systems under static conditions. As a proof of the capability of this system, we studied the effect of four flow rates (i.e., 0, 10, 30, and 50 μL min^{-1}) over the drug release profile in NAA implants infiltrated by Method 1 (i.e. drug loaded on the NAA surface and inside its pores) (Figure 4). A control experiment was performed

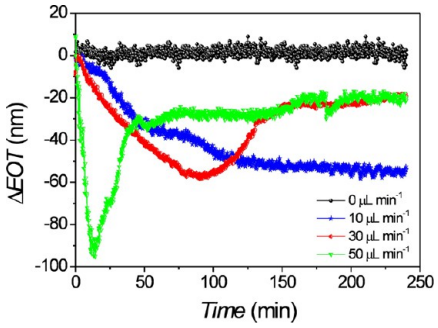

Figure 4. ΔEOT evolution with time for drug release from NAA implants loaded by Method 1 (i.e. drug inside the pores as well as on the surface of the implant) under dynamic conditions at different flow rates from (i.e., from 0 to 50 μL min^{-1}).

under non-flow condition (i.e., 0 μL min^{-1}) and no changes in ΔEOT were observed throughout. This is due to the very small volume of the chamber of our microfuidic device (i.e., 3.6 μL, approximately), which is not big enough to maintain a concentration gradient between the elluting buffer and the drug loaded NAA substrate. A slight decrease in ΔEOT was observed at 10 μL min^{-1}, demonstrating that under these conditions, drug was removed from the NAA surface but not from the pores as a result of the slow flow rate. Nevertheless, experiments performed at 30 and 50 μL min^{-1} presented a triphasic drug release pattern with an initial decrease in ΔEOT (i.e., release of drug molecules from the NAA implant surface) followed by an increase (i.e., release of drug molecules from pores) and a final stationary state (i.e., end of drug release). It was verified that the faster the flow rate, the faster the drug release from both the NAA implant surface and its pores. Furthermore, it was also observed that the ΔEOT peak, which is defined as the transition from the release phases 1 and 2, followed a proportionally reverse trend (i.e. the faster the flow rate the lower the ΔEOT peak), decreasing as: -44 ± 4 nm at 10 μL min^{-1}, -56 ± 3 nm at 30 μL min^{-1}, and -89 ± 7 nm at 50 μL min^{-1}. It is noteworthy that ΔEOT reached its stable value (i.e., release phase 3) faster at 50 μL min^{-1} (i.e., 35 min) than at 30 μL min^{-1} (i.e., 55 min). This result can be explained in terms of buffer exchange rate as the faster the flow rate the faster the buffer solution in the cell chamber was replaced by fresh one (i.e. every 23, 7, and 4 s at 10, 30, and 50 μL min^{-1}, respectively). In other words, the concentration gradient of drug was higher at faster flow rates, increasing the drug release rate as it acts as the driving force of the release process (i.e., diffusion control). These results are in good agreement with previous studies showing that the flow rate affects the drug release from drug loaded polymeric matrices.[23] To the best of our knowledge, this is the first study confirming a similar effect in nanoporous implants based on non-eroding inorganic matrices.

3.4. Release Kinetics: Synergy between Conventional and in Situ Release Monitoring. To establish the relationship between the amount of drug released and the optical thickness change measured at a constant flow rate, we performed a calibration experiment (Figure 5). In this experiment, we related Δ*EOT* with the amount of drug released at certain time, which was established by analyzing the UV-visible spectra of the eluted buffer at the output of the flow cell at 30 μL min^{-1} during the initial release phase (i.e. within the first 100 min of release). ΔEOT and the amount of drug were determined by RIfS and UV-visible spectroscopy, respectively. These were found to be in a good agreement (Figure 5a). Furthermore, as Figure 5b shows, there is a linear relationship between both parameters (i.e. ΔEOT and amount of drug released determined by RIfS and UV−visible spectroscopy, respectively). This result verifies the suitable performance of our optical sensing system to monitor drug release under the aforementioned conditions. Notice that this fast release has been observed in many studies albeit only a few detailed investigations have reported about the release phenomena at this regime, being ignored by most of the mathematical models. Therefore, real-time and in situ monitoring of drug release provides an outstanding advantage over conventional methods as this system makes it possible to collect multiple readings at milisecond time intervals under dynamic conditions. This is crucial to understand the initial fast release of drug from nanoporous implants and it plays an important role in the efficiency of the treatment dependening upon the therapy and drug. Initial fast release could be useful for therapies which require fast release of drug (i.e., wound treatment, inflammation and bacterial infection, etc.). On the other hand, it is not advisable for treatment of conditions that require long-term sustained drug release such as implants (i.e., bone implants, stents, etc.).[17,24,33]

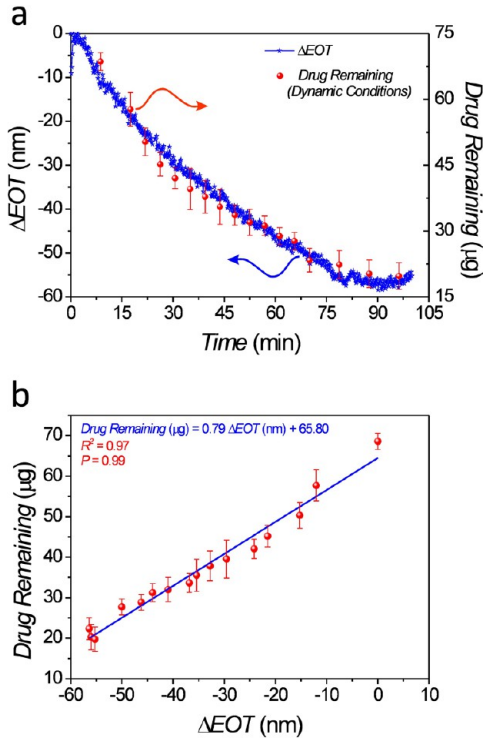

Figure 5. Establishment of relationship between optical thickness and amount of drug released (error bars correspond to standard deviations obtained after averaging 3 measurements). (a) Evolution of ΔEOT at 30 μL min^{-1} and remaining drug inside the NAA pores with time under dynamic conditions established by conventional method. (b) Calibration curve establishing a correlation between the amount of drug remaining and ΔEOT measured during in situ drug release monitoring.

The experimental data obtained from these experiments were fitted to a typical mathematical model for drug delivery kinetics (i.e. Higuchi model).[17,24,34,35] This model, which is based on the Fickian diffusion equation, describes the release of drugs from insoluble matrices. Under such assumptions as perfect sink conditions and significantly higher initial drug concentration in the release platform than in the eluting medium, this model can be used to describe the diffusion-controlled release of water-soluble and poorly water-soluble drugs from inert noneroding porous platforms.

A modified Higuchi equation can be written as eq 1

$$f = \frac{m(t)}{M} = at^{1/2} + b \tag{1}$$

where f is the fraction of drug released, m is the amount of drug released at time t, which can be calculated from ΔEOT, M is the initial amount of drug in the NAA implant determined by TGA, and a and b are fitting parameters.

Therefore, the rate of drug release for this system can be calculated by derivating eq 1. The obtained result shows that the drug release rate is inversly proportional to the square root of time (eq 2).

$$\frac{dM(t)}{dt} = kt^{1/2} \tag{2}$$

where k is the rate constant given by eq 3.

$$k = \frac{1}{2}Ma \tag{3}$$

Table 1 summarizes the rate constant values obtained after fitting the drug release data to the aforementioned Higuchi model from NAA implants obtained under static and dynamic conditions as well as their corresponding R^2 values. The corresponding fitting lines are presented in Figure S4 in the Supporting Information. At first glance, it is observed that the drug release under dynamic conditions at 50 μL min^{-1} is approximately four-fold higher than that obtained under static ones. However, the drug release under dynamic conditions at lower flow rates (i.e., 10 and 30 μL min^{-1}) is comparable to that obtained under static conditions. Notice that the increment of k with the flow rate confirms that the faster the flow rate the higher the amount of drug released from the NAA implants. Furthermore, the high R^2 values verify the $t^{1/2}$ dependence of the drug release, which is a characteristic factor of Fickian diffusion mechanism. These experimental fittings for both methods are in good agreement with the Higuchi model, which justifies our approach for monitoring drug release from nanoporous materials in real-time under dynamic flow conditions by means of reflectometric interference spectroscopy.

4. CONCLUSIONS

To conclude, in this study we have successfully demonstrated the ability of a noneroding and biocompatible platform, nanoporous anodic alumina, to be used as nanoengineered drug eluting implant for biomedical applications. NAA implants were loaded with anti-inflammatory drug indomethacin and their in vitro release profiles were established under static and dynamic conditions by comparative measurements between UV−visible spectroscopy and reflectometric interference spectroscopy. A pronounced difference in drug release time was observed with release extending up to 4 day under static conditions while it lasted only a few hours under dynamic ones. As for this, we studied the effect of the flow rate over the drug release pattern at four different flow rates similar to the physiological milieu at the implant site in the host body. These experimental data were fitted to a modified Higuchi model. Both, experimental data and model fittings verified that the faster the flow rate the higher the amount of released drug. Furthermore, the obtained results suggest that the release mechanism under dynamic conditions was diffusion-controlled.

Table 1. Fit Parameters of the Higuchi Model for the Release of Indomethacin from NAA Implants under Static and Dynamic Flow Conditions at Different Flow Rates

static conditions		dynamic conditions					
		flow rate 10 μL min^{-1}		flow rate 30 μL min^{-1}		flow rate 50 μL min^{-1}	
k (μg min$^{-1/2}$)	R^2	k (μg min$^{-1/2}$)	R^2	k (μg min$^{-1/2}$)	R^2	k (μg min$^{-1/2}$)	R^2
3.02 ± 0.02	0.95	2.23 ± 0.02	0.95	2.80 ± 0.06	0.99	12.47 ± 0.04	0.96

dx.doi.org/10.1021/am4013984 | ACS Appl. Mater. Interfaces 2013, 5, 5436−5442

These results established that to combine dynamic flow conditions with real-time and in situ monitoring of drug release makes it possible to simulate the biological environment at the implant site. The obtained results by this method are more reliable and accurate than those obtained under conventional static conditions. Therefore, we consider this study as an important contribution towards a better understanding of drug release under dynamic conditions, which is crucial to develop more efficient and optimized local drug delivery systems featuring nanoporous layer as drug containers. This approach can be dearly useful to design drug-releasing implants with improved performance and prevent common problems such as infections, lack of integration with surrounding tissues, inflammations, and even total rejection by the host body.

■ ASSOCIATED CONTENT

Supporting Information

Further information about the design of the microfluidic device, determination of drug loading amount, control experiments for confirming the trend of ΔEOT with the different loading methods, and finally, the kinetic model fitting curves for static and dynamic drug release experiments at all the measured flow rates. This material is available free of charge via the internet at http://pubs.acs.org.

■ AUTHOR INFORMATION

Corresponding Author

*E-mail: dusan.losic@adelaide.edu.au.

Author Contributions

The manuscript was written through contributions of all authors. All authors have given approval to the final version of the manuscript.

Notes

The authors declare no competing financial interest.

■ ACKNOWLEDGMENTS

Authors acknowledge the financial support provided by the Australian Research Council (DP 120101680, FT 110100711) and the School of Chemical Engineering − University of Adelaide. We are also thankful to Prof M.J. Sailor (UCSD) for providing FFT analysis software. We thank the Australian National Fabrication Facility (South Australian Node) (ANFF-SA) for the design and fabrication of the microfluidic device.

■ REFERENCES

(1) Langer, R. *Nature* **1998**, *392*, 5−10.
(2) Langer, R. *Science* **2001**, *293*, 58−59.
(3) Jain, J. P.; Modi, S.; Domb, A. J.; Kumar, N. *J. Controlled Release* **2005**, *103*, 541−563.
(4) Porter, J.; Ruckh, T.; Popat, K. *Biotechnol. Prog.* **2009**, *25*, 1539−1560.
(5) Belt, H.; Neut, D.; Schenk, W.; Horn, J. R.; Mei, H. C.; Busscher, H. J. *Acta Orthop.* **2001**, *72*, 557−571.
(6) Lucke, M.; Schmidmaier, G.; Sadoni, S.; Wildemann, B.; Schiller, R.; Haas, N.; Raschke, M. *Bone* **2003**, *32*, 521−531.
(7) Ainslie, K.; Thakar, R.; Bernards, D.; Desai, T. Inflammatory Response to Implanted Nanostructured Materials. In *Biological Interactions on Materials Surfaces*; Puleo, D. A., Bizios, R., Eds.; Springer: New York, 2009; pp 355−371.
(8) Allen, T. M.; Cullis, P. R. *Science* **2004**, *303*, 1818−1822.
(9) Gulati, K.; Aw, M. S.; Findlay, D.; Losic, D. *Ther. Delivery* **2012**, *3*, 857−873.
(10) Liu, H.; Webster, T. *J. Biomater.* **2007**, *28*, 354−369.
(11) Adiga, S. P.; Jin, C.; Curtiss, L. A.; Monteiro-Riviere, N. A.; Narayan, R. J. *WIREs: Nanomed. Nanobiotechnol.* **2009**, *1*, 568−581.
(12) Gulati, K.; Aw, M. S.; Losic, D. *Nanoscale Res. Lett.* **2011**, *6*, 1−6.
(13) Losic, D.; Simovic, S. *Expert Opin. Drug Delivery* **2009**, *6*, 1363−1381.
(14) Maluenda, G.; Lemesle, G.; Waksman, R. *Clin. Pharmacol. Ther.* **2009**, *85*, 474−480.
(15) Gultepe, E.; Nagesha, D.; Sridhar, S.; Amiji, M. *Adv. Drug Delivery Rev.* **2010**, *62*, 305−315.
(16) Popat, K. C.; Eltgroth, M.; LaTempa, T. J.; Grimes, C. A.; Desai, T. A. *Small* **2007**, *3*, 1878−1881.
(17) Gultepe, E.; Nagesha, D.; Casse, B. D. F.; Banyal, R.; Fitchorov, T.; Karma, A.; Amiji, M.; Sridhar, S. *Small* **2009**, *6*, 213−216.
(18) La Flamme, K. E.; Popat, K. C.; Leoni, L.; Markiewicz, E.; La Tempa, T. J.; Roman, B. B.; Grimes, C. A.; Desai, T. A. *Biomaterials* **2007**, *28*, 2638−2645.
(19) Simovic, S.; Losic, D.; Vasilev, K. *Chem. Commun.* **2010**, *46*, 1317−1319.
(20) Aw, M. S.; Addai-Mensah, J.; Losic, D. *Chem. Commun.* **2012**, *48*, 3348−3350.
(21) Aw, M. S.; Addai-Mensah, J.; Losic, D. *J. Mater. Chem.* **2012**, *22*, 6561−6563.
(22) Gulati, K.; Aw, M. S.; Losic, D. *Int. J. Nanomed.* **2012**, *7*, 2069−2076.
(23) Gbureck, U.; Vorndran, E.; Barralet, J. E. *Acta Biomater.* **2008**, *4*, 1480−1486.
(24) Braun, W.; Frommelt, L.; Thull, R. *BIOmaterialien* **2011**, *7*, 286−290.
(25) Hall, E. W.; Rouse, M. S.; Jacofsky, D. J.; Osmon, D. R.; Hanssen, A. D.; Steckelberg, J. M.; Patel, R. *Diagn. Microbiol. Infect. Dis.* **2004**, *50*, 261−265.
(26) Perry, A. C.; Rouse, M. S.; Khaliq, Y.; Piper, K. E.; Hanssen, A. D.; Osmon, D. R.; Steckelberg, J. M.; Patel, R. *Clin. Orthop. Relat. Res.* **2002**, *403*, 49−53.
(27) Kumeria, T.; Kurkuri, M. D.; Diener, K. R.; Parkinson, L.; Losic, D. *Biosens. Bioelectron.* **2012**, *35*, 167−173.
(28) Kumeria, T.; Losic, D. *Physica Status Solidi (RRL)* **2011**, *5*, 406−408.
(29) Kumeria, T.; Parkinson, L.; Losic, D. *Nanoscale Res. Lett.* **2011**, *6*, 1−7.
(30) Alvarez, S. D.; Li, C. P.; Chiang, C. E.; Schuller, I. K.; Sailor, M. J. *ACS Nano* **2009**, *3*, 3301−3307.
(31) Kumeria, T.; Losic, D. *Nanoscale Res. Lett.* **2012**, *7*, 88−97.
(32) Masuda, H.; Fukuda, K. *Science* **1995**, *268*, 1466−1468.
(33) Huang, X.; Brazel, C. S. *J. Controlled Release* **2001**, *73*, 121−136.
(34) Siepmann, J.; Siepmann, F. *Int. J. Pharm.* **2008**, *364*, 328−343.
(35) Arifin, D. Y.; Lee, L. Y.; Wang, C. H. *Adv. Drug Delivery Rev.* **2006**, *58*, 1274−1325.